Quang VU DUC[1*]

A COMPARATIVE SIMULATION STUDY ON SPRINGBACK AND FORMABILITY OF SQUARE CUPS: HYDROMECHANICAL VS. CONVENTIONAL DEEP DRAWING

This paper presents a comparative simulation study on springback and formability in square cup manufacturing using Conventional (CDD) and Hydromechanical Deep Drawing (HMDD). While CDD relies on mechanical force, HMDD employs controlled fluid pressure, offering advantages like reduced friction, suppressed wrinkling, and higher formability. Using Abaqus/CAE, 3D models simulated the entire forming and springback process for two specimens: C1 (CDD) and C2 (HMDD). Effectiveness was evaluated based on six criteria: the forming process, Von Mises stress, residual stress, equivalent plastic strain, thickness distribution, and springback magnitude along OX, OY, and OZ axes. Results show HMDD produces superior quality. Specimen C2 exhibits more uniform stress and strain distribution, better-controlled thinning, and crucially, a significantly minimized springback (especially OZ-axis displacement at the flange and bottom corners), reduced by up to 2.5 times. This confirms HMDD's effectiveness for manufacturing precise, complex box-shaped components. The study provides a valuable database and methodology for optimizing processes and controlling defects in automotive, aerospace, and machinery manufacturing.

1. INTRODUCTION

Metal square cup components are crucial mechanical parts widely used in industries such as automotive, aerospace, oil and gas, etc. Producing them with high precision and stable quality remains a significant technical challenge, primarily due to their complex geometry leading to uneven strain distribution and, particularly, the springback phenomenon after forming. The CDD process is widely used due to its simplicity and lower initial investment cost. However, it suffers from inherent drawbacks such as high friction causing tool wear, significant risks of wrinkling and tearing, a low Limiting Drawing Ratio (LDR), and, most critically, difficulty in controlling springback, which leads to part shape deviation [1]. To overcome these limitations, HMDD has been developed as an advanced solution. In the

HMDD process, fluid pressure is used to replace or assist the female die, offering superior advantages like significantly reduced friction, improved formability (higher LDR), suppression of wrinkling and tearing, and better surface quality [2]. Nevertheless, HMDD requires a more complex hydraulic system, higher investment and maintenance costs, and the optimization of the fluid pressure curve is crucial for achieving optimal results [3, 4].

The Finite Element Method (FEM) has proven to be a powerful and cost-effective tool for analysing, simulating, and optimizing complex sheet metal forming processes. For both CDD and HMDD processes, FEM enables researchers to accurately predict defects (such as wrinkling, tearing, springback), stress-strain distribution, and thickness variation without conducting numerous expensive trials [5, 6]. Commercial software like Abaqus, with its Explicit module for simulating the dynamic forming process and Standard module for static springback analysis, has been widely used and its reliability validated through comparison with experimental results [7].

The HMDD process continues to be researched and developed as a superior solution for enhancing the formability and accuracy of complex sheet metal components. Recent studies focus on process optimization, defect control, and outcome prediction. Specifically, Amini et al. [8] demonstrated that fluid pressure, pre-bulge height, and friction are key parameters for effectively controlling surface wrinkling when forming conical components, thereby proposing process enhancements. A fundamental advantage of HMDD was confirmed by Ballikaya et al. [9] through achieving a high LDR, attributed to reduced friction and improved stress distribution.

To further enhance microstructural quality and formability, Ghasemi et al. [10] demonstrated the effectiveness of integrating radial ultrasonic vibration into the punch within an HMDD die, significantly improving product microstructural homogeneity. Regarding the control of springback – a major challenge for geometric accuracy - experimental studies by Hiseeb & Khleif [11] on low-carbon AISI 1008 steel showed that holding time and fluid pressure are two decisive factors influencing the degree of springback. In the context of optimizing the process for specific shapes, Jaber et al. [12] conducted experimental investigations into the technological parameters of the hydrostatic forming method to enhance the formability of a steel square cup. Parallel to experimental research, the trend of applying artificial intelligence for process prediction and optimization is emerging strongly, as evidenced by the study of Gu et al. [13] developing a Transfer Learning method to predict deep drawing force with high accuracy and low computational cost. In summary, these advanced studies not only reinforce the inherent advantages of HMDD but also open diverse approaches, from optimizing technological parameters and integrating auxiliary techniques (ultrasonics) to applying intelligent predictive tools, aiming for the ultimate goal of producing high-quality components with optimal accuracy.

Springback remains a critical challenge in the sheet metal deep drawing process, directly affecting the dimensional accuracy and quality of the formed part. Recent studies have extensively analyzed the factors influencing this phenomenon, highlighting the complexity of its prediction and control. A foundational study by Lal et al. [14] systematized the key factors, including material properties, tool geometry, and process parameters such as blank holder force and friction. The critical role of material modeling was emphasized by Vallaster et al. [15], who showed that incorporating strain rate dependence in the material law for advanced

high-strength steel significantly improves the predictive accuracy of finite element simulations for both forming force and springback. This is particularly important when processing advanced materials, as studies on high-strength steel and high-strength aluminum alloys confirm their significantly greater susceptibility to springback compared to conventional grades [16]. Rigas et al. [17] further found that the forming method itself (e.g., deep drawing vs. fluid-based forming) creates different stress states and consequently leads to varying degrees of springback even for the same aluminum alloy. To mitigate these issues at the process design stage, innovative approaches such as workpiece-performance-based design of multi-step dies have been proposed, promising more uniform strain distribution and potential springback reduction [18]. In conclusion, contemporary research agrees that accurate springback prediction requires sophisticated material models, careful selection of forming strategies for advanced materials, and innovative die design. However, a comprehensive analysis comparing conventional deep drawing and hydromechanical deep drawing, with a focused evaluation of residual stress, plastic strain distribution, and multi-axis springback displacement, remains a gap needing investigation for complex-geometry components like square cups.

This paper presents an analysis based on Abaqus/Explicit simulation to compare the square cup formability between the two processes, CDD (forming specimen C1) and HMDD (forming specimen C2), and based on Abaqus/Standard simulation to compare springback for ensuring accuracy [19]. The study focuses on a comprehensive evaluation and comparison through six key criteria: the forming process, distribution of Von Mises forming stress within the component, distribution of residual stress, distribution of the equivalent plastic strain at integration points, material thickness distribution, and the magnitude of springback along the three axes OX, OY, and OZ. The results of this study provide in-depth insights and valuable reference for engineers and researchers in selecting and optimizing technological processes, aiming for practical application in manufacturing precise sheet metal components, especially in fields demanding high reliability like the automotive and aerospace industries.

2. MATERIALS AND METHODS

2.1. SHEET BLANK AND DIE MODELS

The blank material for forming specimens C1 and C2 is SUS304 stainless steel, with mechanical properties presented in table 1. The geometric model of the blank is square-shaped with side dimensions $a_b = 200$ mm and an initial thickness $t_0 = 1$ mm, as shown in Fig. 1a. The mesh model of the blank is shown in Fig. 1b and configured for simulation as detailed in Table 2. The punch has side dimensions $a_p = 100$ mm, a height $h_p = 70$ mm, with its edges and tip filleted to a radius $R_f = 10$ mm. The die has a cavity with side dimensions $a_d = 102.5$ mm, a depth $h_d = 78.75$ mm, and transition corners filleted to the same radius $R_f = 10$ mm. The blank holder is designed to be compatible with the die and punch, with a clearance of 1.25 mm between them. The key dimensions of the two square cup specimens, C1 and C2, are as follows: the punch-side length $a_C = a_p = 100$ mm, the cup depth $H_C = H_{OZ} = 45$ mm,

and the fillet radius $R_C = R_f = 10$ mm. The model setups for the two forming processes are illustrated in Fig. 2 and Table 2.
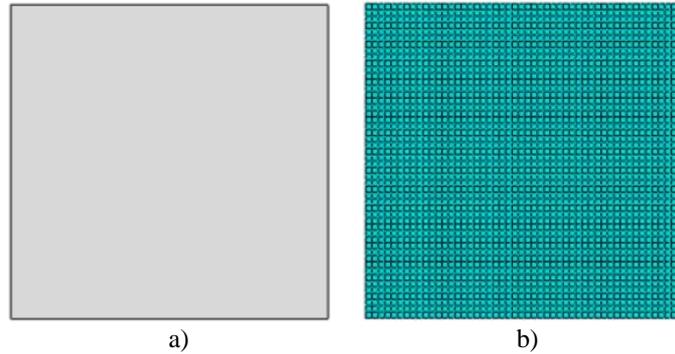

a)   b)

Fig. 1. SUS304 sheet blank setup: a) Geometric model, b) Mesh model

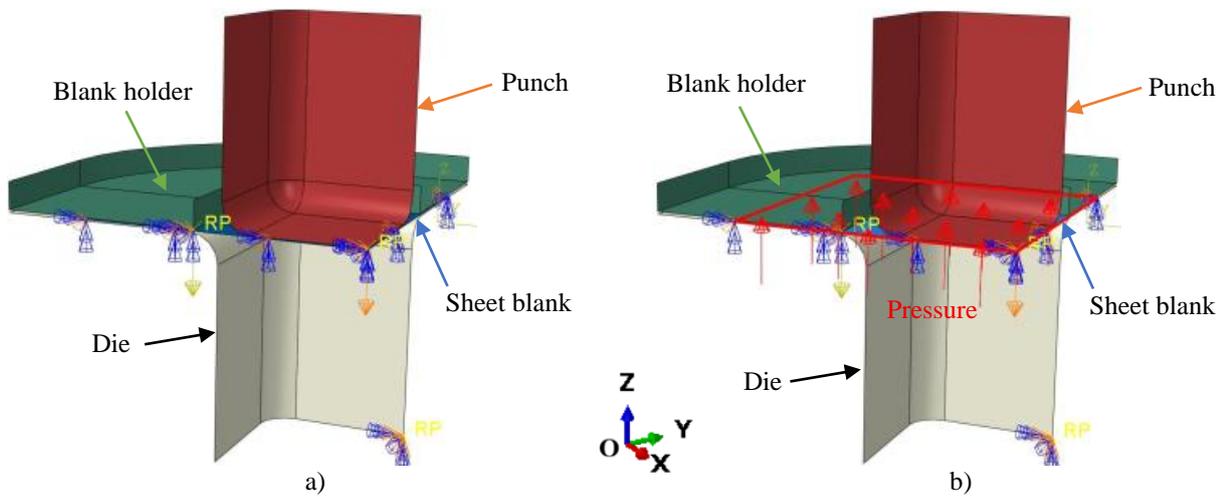a)   b)

Fig. 2. Setup of the two forming process models: a) CDD process, b) HMDD process

Table 1. The material properties of SUS304 sheet blank

Material properties of the SUS304 sheet blank	Value
Temperature (ºC)	24
Density, ρ (kg/m³)	7850
Young's modulus, E (GPa)	193
Hardening coefficient, K (MPa)	1275
Work hardening exponent, n	0.45
Poisson's ratio, v	0.29
Yield strength, σ_Y (MPa)	226.3
Ultimate tensile strength, σ_U (MPa)	566.0
Elongation (%)	50.0

2.2. FE SIMULATION

The FE simulation setup for the two processes, CDD and HMDD, to form specimens C1 and C2 was established in Abaqus/CAE using the Dynamic, Explicit models and configurations presented in Fig. 2 and Table 2. Boundary conditions common to both processes include a friction coefficient of 0.125 between the sheet blank and the die. The contact between the blank and the holder uses the default "hard" contact property model in Abaqus/Explicit, which assumes frictionless, no thermal interaction, etc., in the normal direction. The punch displacement follows the load curve Amp-1 (Smooth step), and the blank holder is modeled as applying a concentrated force of 22870 N. An additional boundary condition of fluid pressure with a value of $P_{HMDD} = 5$ MPa inside the die cavity was set for the HMDD process.

Table 2. Simulation setup for the two processes

Name	Modeling Space	Type	Basic feature (Shap)	Mesh (1/4 model) and Boundary condition
Forming (Dynamic, Explicit) - CDD and HMDD Process				
SUS304Sheetblank	3D	Deformable	Shell	2500 elements, type = S4D - Explicit
Punch	3D	Discrete rigid	Shell	328 elements, type = R3D4 - Explicit. - OZ axis displacement: $H_{OZ} = -45$ mm.
Die	3D	Discrete rigid	Shell	432 elements, type = R3D4 - Explicit. - Fixed.
Blankholder	3D	Discrete rigid	Shell	144 elements, type = R3D4 - Explicit. - Fixed.
Springback (Static, General) - Subsequent Step of the CDD and HMDD Process				
SUS304Sheetblank	3D	Deformable	Shell	2500 elements, type = S4D - Explicit.

The FE simulation for springback after completing the CDD and HMDD processes was set up using the same geometric and mesh models of the sheet blank. The configuration employed the Static, General procedure as detailed in table 2.1, with the boundary conditions applied as shown in Fig. 3.
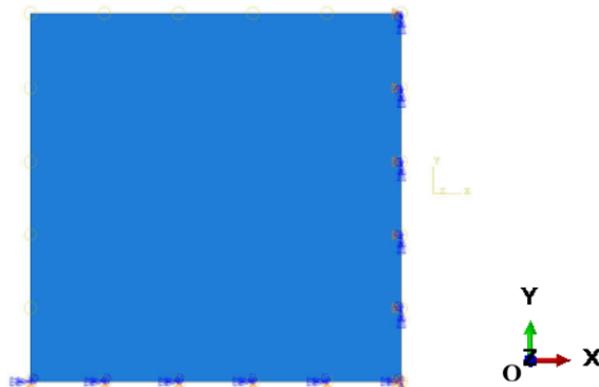

Fig. 3. Boundary conditions set for the springback simulation

3. RESULTS AND DISCUSSION

3.1. FORMING PROCESSES

The punch force applied to the sheet blank ($F_{p\text{-}CDD}$) during the punch stroke in the Conventional Deep Drawing process (Fig. 4d) is lower than the punch force ($F_{p\text{-}HMDD}$) applied during the punch stroke in the HMDD process (Fig. 5d). Both forces reach their maximum values at a stroke depth of $H_{OZ} = -22.5$ mm, with $F_{p\text{-}HMDDmax} = 46652.8$ N $> F_{p\text{-}CDDmax} = 32477.2$ N. The punch forces then decrease to $F_{p\text{-}HMDD} = 33101.1$ N and $F_{p\text{-}CDD} = 22036.1$ N upon completion of the punch stroke at $H_{OZ} = -45.0$ mm, resulting in the two formed specimens shown in Fig.s 4c and 5c.

The load curves in Fig.s 4d and 5d demonstrate that the punch force evolution in both forming processes is appropriate. The fluid pressure acting on the lower surface of the blank in the HMDD process causes the punch force $F_{p\text{-}HMDD}$ to consistently exceed the punch force $F_{p\text{-}CDD}$ in the CDD process throughout the stroke. Notably, the punch force variation is smoother in the first half of the stroke for the CDD process compared to the HMDD process. Conversely, the force variation becomes smoother in the second half of the stroke for the HMDD process compared to the CDD process.

A significant and observable difference occurs in the initial second of each forming process. In the HMDD process, the fluid pressure from the die cavity causes the blank to bulge upward and conform closely to the punch's tip fillet radius (Fig. 5a). In contrast, the blank in the CDD process remains nearly horizontal (Fig. 4a). At the end of the punch stroke ($H_Z = -45.0$ mm), an advantage of the HMDD process is evident: the resulting fillet radius at the cup flange of specimen C2 (Fig. 5b) is smaller than that of specimen C1 (Fig. 4b).

a)   b)

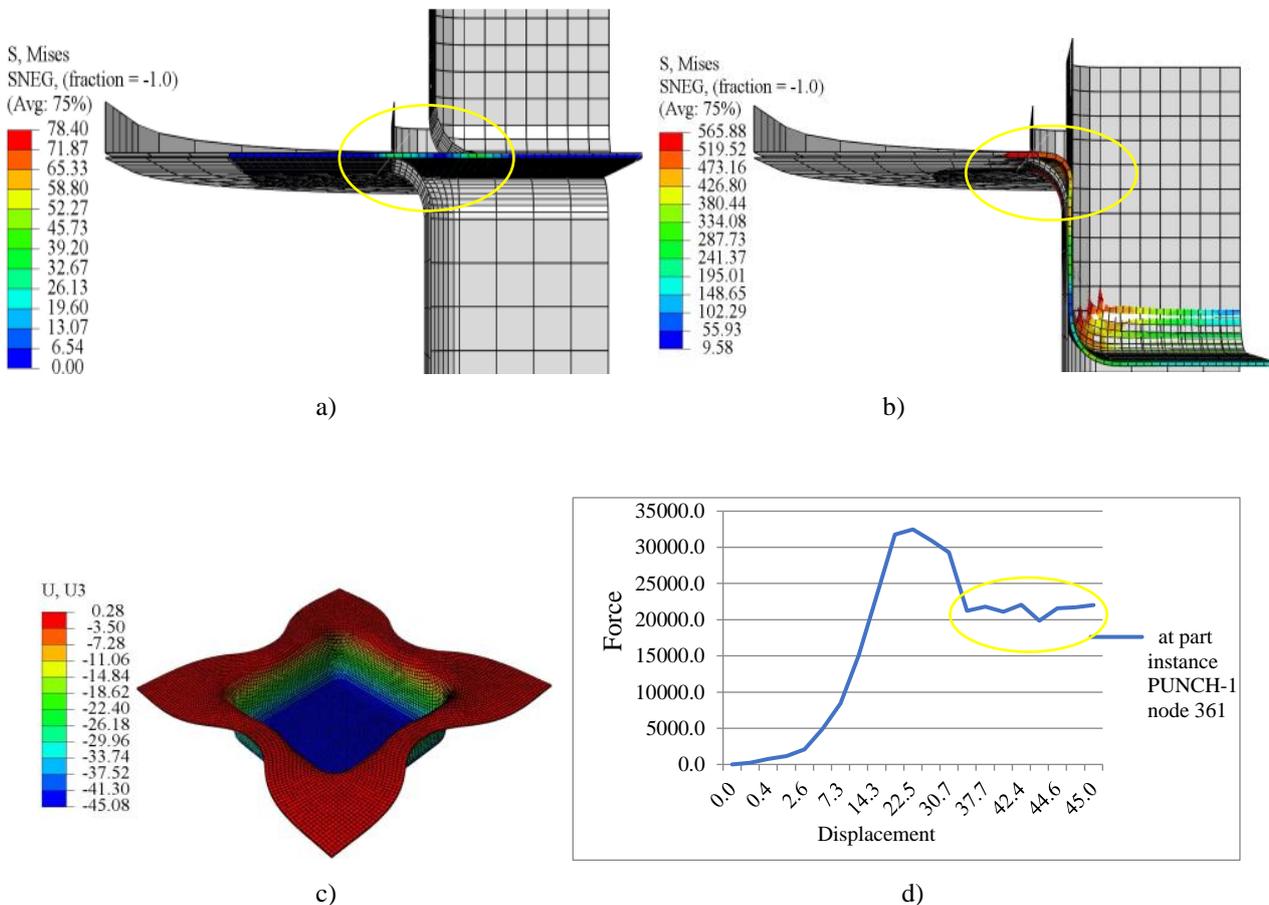c)   d)

Fig. 4. CDD process forming specimen C1: a – Initial stage when the punch first contacts the blank, b – End of the punch stroke, c – Formed specimen, d – Applied punch load curve versus punch stroke
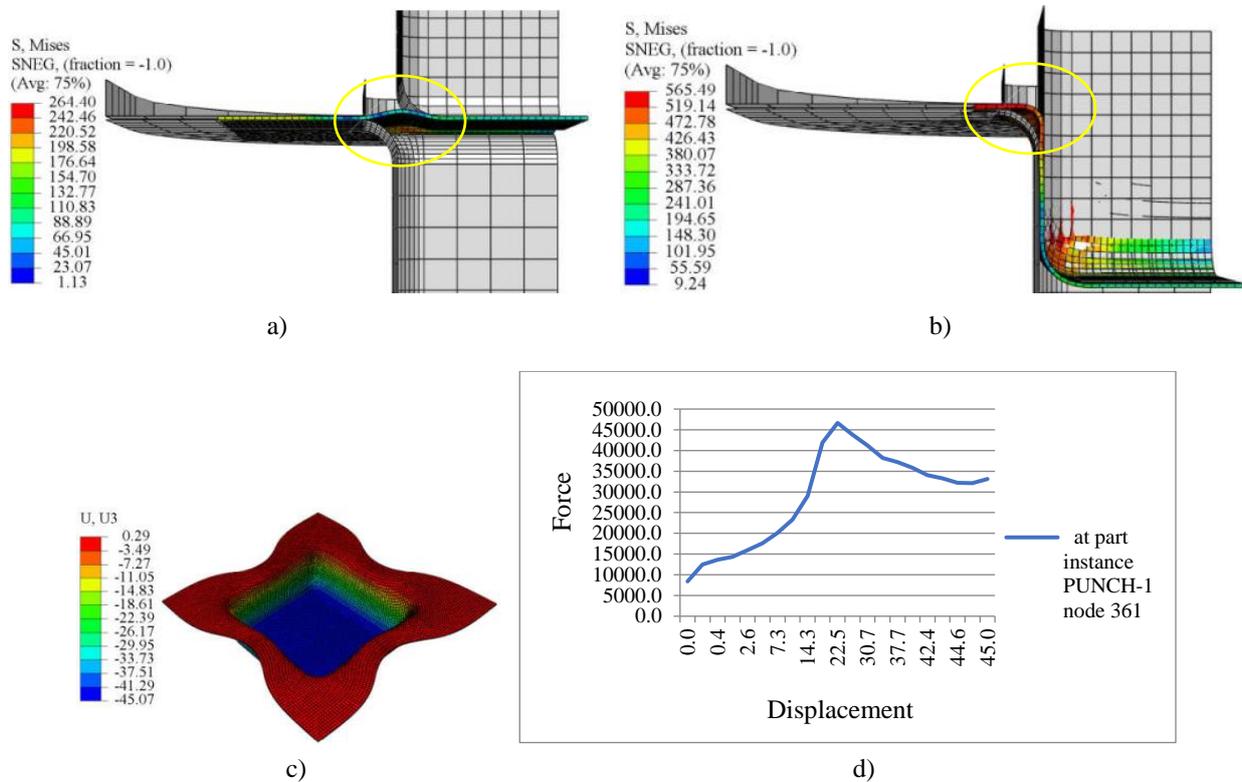

a)   b)

c)   d)

Fig. 5. HMDD process forming specimen C2: a – Initial stage when the punch first contacts the blank, b – End of the punch stroke, c – Formed specimen, d – Applied punch load curve versus punch stroke

3.2. FORMING STRESS AND RESIDUAL STRESS

The distribution of forming stress and residual stress in specimens C1 and C2 is presented in Fig. 6. The distribution of S_{C1} (Fig. 6a) is similar to that of S_{C2} (Fig. 6c), with maximum values of S_{C1-max} = 565.88 MPa ≈ S_{C2-max} = 565.49 MPa. These high stresses are distributed across broad areas primarily at the four rounded corners and the flange of the cup, approximately equal to the material's ultimate tensile strength, σ_U = 566.0 MPa. The cup walls and the four side panels of both specimens $C1$ and $C2$ also exhibit similar forming stress distributions, with value ranges of S_{C1} = 9.58 MPa to 473.16 MPa and S_{C2} = 9.24 MPa to 472.78 MPa. A notable difference in forming stress distribution occurs in the cup bottom region. Specimen $C2$ shows a uniform stress value of S_{C2} = 287.36 MPa across the bottom, whereas in specimen $C1$, the stress increases from the center towards the transition fillet radius to the wall, ranging from S_{C1} = 148.65 MPa to 334.08 MPa.

The residual stress distribution also shows similar spatial patterns in both specimens $C1$ (Fig. 6b) and $C2$ (Fig. 6d), differing mainly in their magnitude ranges. The four regions located between the square side walls, near the transition fillet to the flange, in both specimens exhibit the highest residual stress (represented by the red color scale): $S_{C1-Rmax}$ = 483.188 MPa

(where $\Delta S_{C1\text{-}Rmax} = \sigma_U - S_{C1\text{-}Rmax} = 566.0 - 483.18 = 82.82$ MPa) and $S_{C2\text{-}Rmax} = 504.56$ MPa (where $\Delta S_{C2\text{-}Rmax} = \sigma_U - S_{C2\text{-}Rmax} = 566.0 - 504.56 = 61.44$ MPa). This data indicates that $S_{C2\text{-}Rmax}$ is greater than $S_{C1\text{-}Rmax}$ by a value of $\Delta S = 504.56 - 483.18 = 21.38$ MPa. The lowest residual stress is found in the cup bottom region of both $C1$ and $C2$; however, the residual stress in specimen $C1$ is more uniform ($S_{C1\text{-}Rmin} = 2.57$ MPa) compared to that in specimen $C2$ ($S_{C2\text{-}Rmin} = 5.15$ MPa). Another difference is observed at the four rounded corners near the cup bottom of specimen $C1$ (Fig. 6b), where two points reach the maximum residual stress value of $S_{C1\text{-}Rmax} = 483.188$ MPa, attributed to the complex stress re-distribution state during the CDD process.
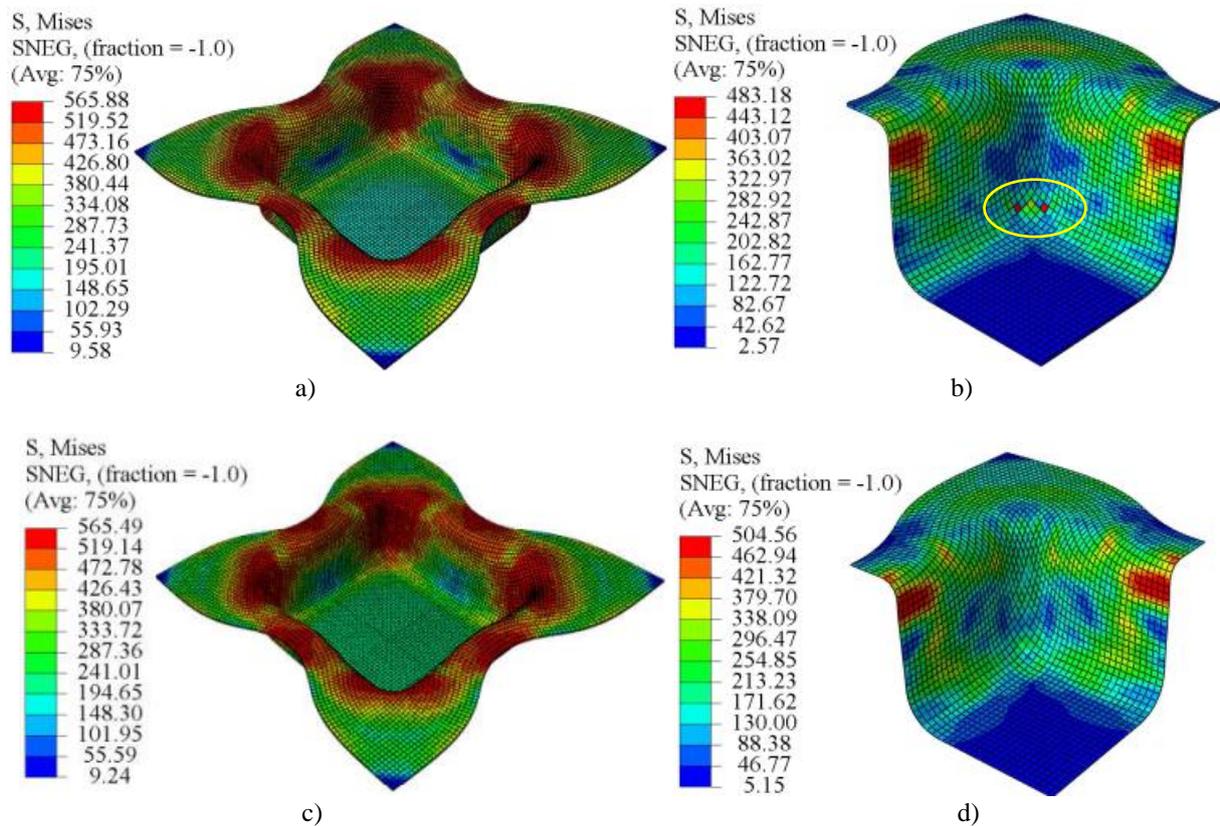

Fig. 6. Stress distribution in specimens C1 and C2: a - Forming stress S_{C1}, b - Residual stress $S_{C1\text{-}R}$, c - Forming stress S_{C2}, d - Residual stress $S_{C2\text{-}R}$

3.3. EQUIVALENT PLASTIC STRAIN AT INTEGRATION POINTS

The distribution of equivalent plastic strain at integration points (PE) at the end of the CDD and HMDD forming processes and after springback in specimens $C1$ and $C2$ is shown in Fig. 7. The distribution PE_{C1} (Fig. 7a) is similar to PE_{C2} (Fig. 7c). Areas subjected to significant plastic deformation are primarily concentrated at the four rounded corners and the nearby cup flange. The maximum values are $PE_{C1\text{-}max} = 0.77$ and $PE_{C2\text{-}max} = 0.53$, located mainly at the four rounded corners near the flange. Both are below the safe limit $[PE_{max}] = 1.0$. The HMDD process demonstrates a clear advantage in terms of a more

favorable plastic strain distribution compared to CDD. The cup bottom and the four side panels of both specimens show very similar, minimal PE distributions, with values ranging from 0.00 to 0.09, indicating that the blank material underwent very little or no plastic deformation in these areas.

A distinct difference in PE distribution is observed between specimens $C1$ (Fig. 7b) and $C2$ (Fig. 7d) after springback. However, since the values are very low ($PE_{C1\text{-Smax}} = PE_{C2\text{-Smax}} = 0.01 \ll 1.0$), this difference has negligible impact on the final forming results of both processes. Specifically, the distribution in $C1$ shows a $PE_{C1\text{-Smax}} = 0.1$ concentrated in a small area at a rounded corner near the transition radius to the cup bottom, represented by seven color scale gradations (Fig. 7b). This is caused by the concentrated residual stress $S_{C1\text{-Rmax}} = 483.188$ MPa in this region (Fig. 6b). Similarly, the distribution in $C2$ shows a $PE_{C2\text{-Smax}} = 0.1$ concentrated in a small area at a rounded corner, represented by five red color nodes (Fig. 7d). This local concentration results from a complex forming stress state in that area during HMDD, even though the residual stresses there are lower, ranging from $S_{C2\text{-R}} = 46.77$ MPa to 296.47 MPa (Fig. 6b).
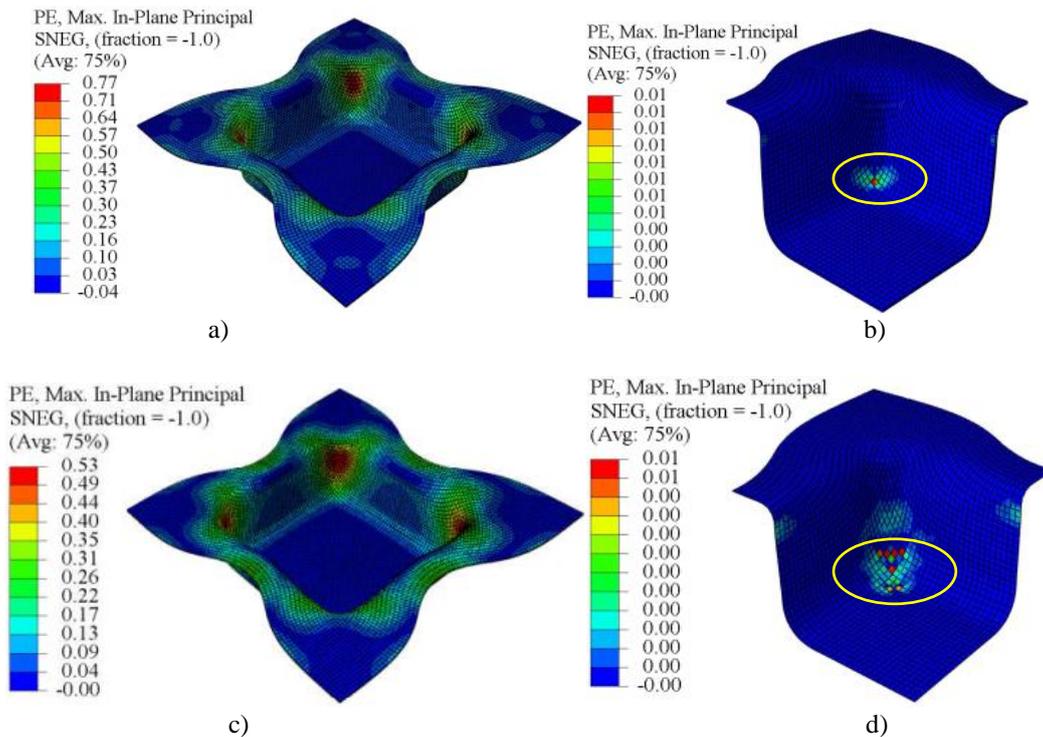

Fig. 7. Equivalent plastic strain at integration points in specimens $C1$ and $C2$: a - Equivalent plastic strain at integration points at the end of the CDD forming process PE_{C1}, b - Equivalent plastic strain at integration points after springback $PE_{C1\text{-S}}$, c - Equivalent plastic strain at integration points at the end of the HMDD forming process PE_{C2}, d - Equivalent plastic strain at integration points after springback $PE_{C2\text{-S}}$

3.4. MATERIAL THICKNESS DISTRIBUTION ON THE SPECIMENTS

The material thickness distribution on the two specimens, STH_{C1} (Fig. 8a) and STH_{C2} (Fig. 8b), is one of the most important criteria reflecting forming quality. The cup flange,

wall, and bottom regions show similarities in material thickness. Due to a complex three-dimensional stress state combining tensile and compressive stresses at the cup flange, the material is compressed to feed into the die cavity. The most severe thickening occurs in small areas such as the region between two side panels and near the rounded corners, reaching $STH_{C2-max} = 1.22$ mm $\approx STH_{C1-max} = 1.23$ mm (thickening ratio $\varepsilon_{max} = 22\%$ to 23%). The cup bottom region of specimen $C1$ (under a biaxial stress state) and C2 (under a triaxial stress state) has a thickness nearly unchanged from the initial blank thickness, with $STH_{C1} \approx STH_{C2} \approx t_0 = 1.0$ mm.
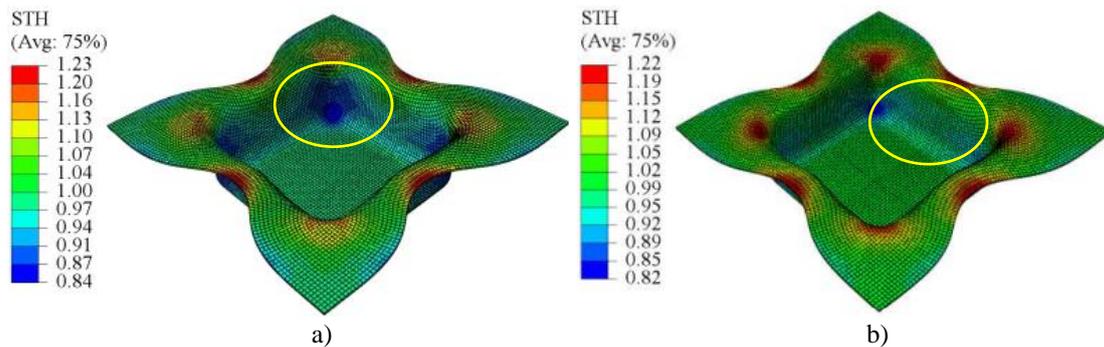

Fig. 8. Material thickness distribution in specimens C1 and C2: a - STH_{C1}, b - STH_{C2}

The most significant difference is evident in the cup walls and rounded corners. The triaxial stress state in the cup wall of specimen $C2$ results in a uniform STH_{C2} distribution (dominated by the green color scale) with a value range from 0.89 mm to 0.99 mm. In contrast, the biaxial tensile stress state in the cup wall of specimen $C1$ leads to an STH_{C1} distribution ranging from 0.84 mm to 0.97 mm. Specimen C1 experiences the most severe thinning across all four rounded corners, with $STH_{C1-min} = 0.84$ mm and a thinning ratio $\varepsilon_{C1-min} = -16\% > [\varepsilon_{min}] = -30\%$ [20]. Meanwhile, the four rounded corners of specimen $C2$ also experience significant thinning but are concentrated in a small area near the cup bottom, with $STH_{C2-min} = 0.82$ mm and a thinning ratio $\varepsilon_{C2-min} = -18\% > [\varepsilon_{min}] = -30\%$.

3.5. SPRINGBACK ALONG THE 3 AXES OX, OY, AND OZ

Springback alters the shape of the previously formed specimens $C1$ (Fig. 4c) and $C2$ (Fig. 5c). Figures 9 and 10 show the results of springback along the 3 axes OX, OY, and OZ after the tools have been removed and the fluid pressure ($P_{HMDD} = 5$ MPa) has been released to zero. The springback of the cup wall along the OX and OY axes is comparable for both specimens $C1$ and $C2$. For specimen $C1$, Fig.s 9a and 9b show that springback causes the cup wall to curve inward toward the cup interior along the OX axis (with four color gradations from yellow to red in Fig. 9a) and the OY axis (with four color gradations from light blue to navy blue in Fig. 9b). They have a maximum springback displacement value of $U1_{C1-OX-max} = U2_{C1-OY-max} = 0.16$ mm. Similarly, for specimen $C2$, Fig.s 10a and 10b show $U1_{C2-OX-max} = U2_{C2-OY-max} = 0.17$ mm.

Examining springback along the OZ axis for specimen *C*1 (Fig.s 9c and 9d) and *C*2 (Fig.s 10c and 10d) clearly reveals the advantage of HMDD over CDD at the cup flange region and the bottom corner fillet region. Springback affects the entire cup flange, represented by 12 color gradations for both specimen *C*1 (Fig. 9c) and specimen *C*2 (Fig. 10c). This shows that the tips of the four petals (corresponding to the four corners of the square cup) are most significantly affected, with a value of $U3_{C1\text{-}OZ\text{-}max} = 1.22$ mm ≈ 2.5 $U3_{C2\text{-}OZ\text{-}max}$ for specimen *C*2. In the bottom corner fillet region, specimen *C*1 also exhibits a springback displacement approximately 2.5 times greater than that in specimen *C*2.

This analysis shows that while springback along the OX and OY axes is comparable between the two methods, HMDD demonstrates a superior advantage in controlling and minimizing springback along the OZ axis, particularly at sensitive regions like the cup flange and bottom corners, thereby achieving higher geometric accuracy compared to the CDD method.
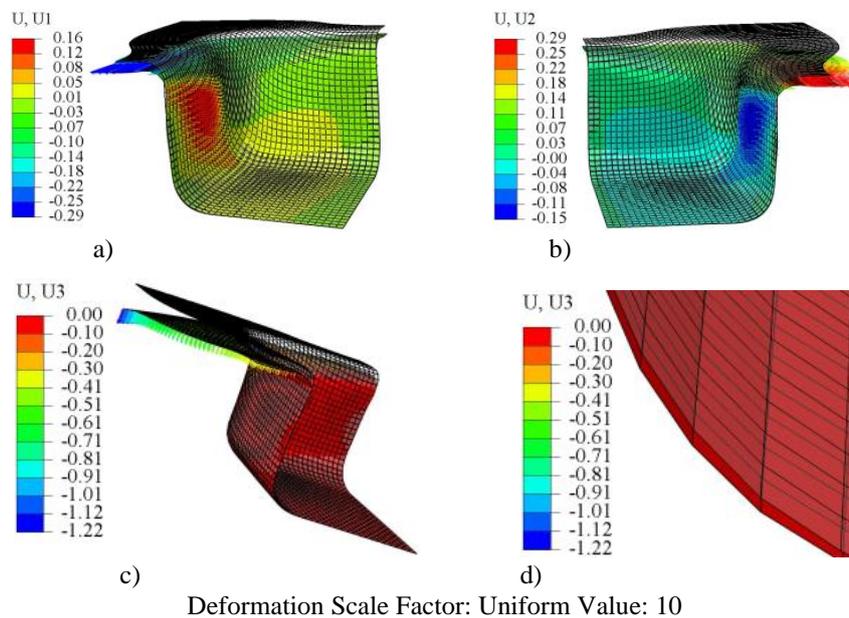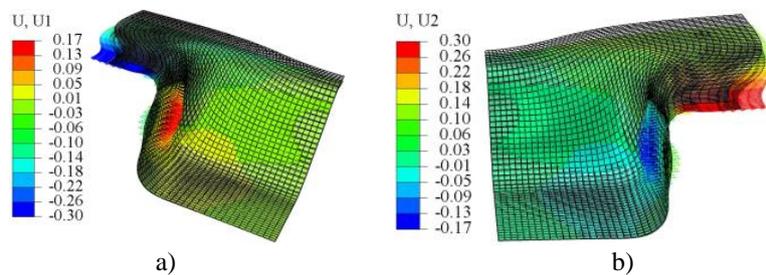

Deformation Scale Factor: Uniform Value: 10

Fig. 9. Springback along 3 axes in specimen C1: a – Along the OX axis, b – Along the OY axis, c and d – Along the OZ axis
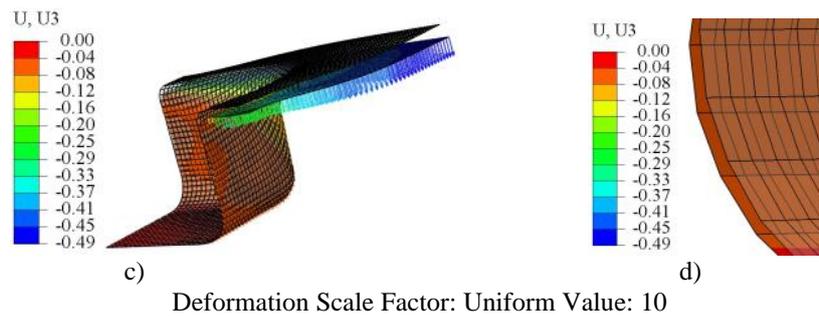
Deformation Scale Factor: Uniform Value: 10

Fig. 10. Springback along 3 axes in specimen *C*2: a – Along the OX axis, b – Along the OY axis, c and d – Along the OZ axis

4. CONCLUSION

Unlike previous studies focusing solely on the formability of square cups via either conventional deep drawing or hydromechanical deep drawing in isolation, this study has successfully conducted a comprehensive, simulation-based comparative analysis of the formability and springback phenomenon between these two processes by systematically evaluating six key criteria. From the analysis results, the following main conclusions can be drawn:

- The simulation process demonstrates that HMDD allows for more stable control of the forming process. The fluid pressure acts as an active controller, helping to limit defects such as surface wrinkling and material tearing, which are common challenges in CDD.

- The HMDD method produces a significantly more uniform and optimal distribution of forming stress in specimen *C*2 compared to the stress distribution in specimen *C*1 from the CDD method. Due to the supporting mechanism of the fluid pressure (P_{HMDD} = 5 MPa), the residual stress in the HMDD-formed specimen is markedly lower by $\Delta S = 504.56 - 483.18 = 21.38$ MPa, contributing to improved dimensional stability and a reduction in stored elastic deformation energy.

- The distribution of PE_{C2}, ranging from 0.00 to 0.53, is smaller than that of PE_{C1}, which ranges from –0.04 to 0.77. This indicates that the material in the HMDD method undergoes deformation more effectively across the entire component surface, in contrast to the localized strain concentration at corners and side walls typically observed in the CDD method.

- The HMDD process demonstrates a superior advantage in controlling the material thickness distribution (STH). Specimen *C*2, formed by the HMDD process, experiences less severe thickness reduction, particularly in the transition corner regions. These areas are subject to a complex stress-strain state and are prone to localized thinning in specimen *C*1, which was formed by the CDD process.

- Reduced susceptibility to springback is one of the most prominent advantages of the HMDD process compared to the CDD process. The springback displacements along the OX and OY axes are equivalent after the forming step of both processes, with $U1_{C1\text{-}OX\text{-}max} = U2_{C1\text{-}OY\text{-}max} = 0.16$ mm and $U1_{C2\text{-}OX\text{-}max} = U2_{C2\text{-}OY\text{-}max} = 0.17$ mm. However, following the HMDD process, the influence of springback is significantly minimized along the OZ axis, with $U3_{C2\text{-}OZ\text{-}max} = 0.49$ mm $\approx 0.4 U3_{C2\text{-}OZ\text{-}max}$. This further confirms that the HMDD process

produces components with higher geometric accuracy than the CDD process after tool removal and the release of fluid pressure (P_{HMDD} = 5 MPa to zero). This method promises high technical and economic efficiency for manufacturing industries that demand high precision, such as the automotive and aerospace sectors.

REFERENCES

[1] ZEIN H., et al., 2014, *Thinning and Spring Back Prediction of Sheet Metal in the Deep Drawing Process*, Mater. Des., 53, 797–808.

[2] BELL C., et al., 2020, *A State of the Art Review of Hydroforming Technology: Its Applications, Research Areas, History, and Future in Manufacturing*, Int. J. Mater. Form., 13, 789–828.

[3] KIMURA S., FURUSHIMA T., 2023, *New Small-Scale Hydromechanical Deep-Drawing Process Using Die-Integrated Active High-Pressure Generation System*, Int. J. Mater. Form., 16/46, 1–11.

[4] NIELSEN C.V., MARTINS P.A.F., 2021, *Metal Forming: Formability, Simulation, and Tool Design*, 1st ed. London, England, Academic Press – Elsevier Inc.

[5] CHOUDHARI C.S., KHASBAGE S.S., 2021, *Experimental Investigation of Forming Parameters for Square Cup Deep Drawing Process*, Mater. Today Proc., 44/6, 4261–4267.

[6] SUN Z., LANG L., 2017, *Effect of Stress Distribution on Springback in Hydroforming Process*, Int. J. Adv. Manuf. Technol., 93, 2773–2782.

[7] QUANG V.D., 2025, *The Optimization of Rotary Bending Die Process: Criteria for the Metal Sheet Angles and Springback Effects*, Eng. Technol. Appl. Sci. Res., 15/1, 20553–20558.

[8] AMINI A., et al., 2025, *Hydro-Mechanical Deep Drawing of Conical Components: Wrinkling Behavior and Process Enhancement*, Journal of Engineering Research, 13/2, 975–984.

[9] BALLIKAYA H., SAVAS V., OZAY C., 2020, *The Limit Drawing Ratio in Die Angled Hydromechanical Deep Drawing Method*, Int. J. Adv. Manuf. Technol., 106, 791–801.

[10] GHASEMI R., ELYASI M., BASERI H., et al., 2023, *Microstructural Analysis of Sheet Hydroforming Process Assisted by Radial Ultrasonic Punch Vibration in Hydro-Mechanical Deep Drawing Die*, Int. J. Adv. Manuf. Technol., 125, 5359–5368.

[11] HIBAT ALLAH J., HISEEB A.A.K, 2024, *Experimental Investigations of a Springback in Hydromechanical Deep Drawing of Low Carbon Steel 1008 AISI*, Tikrit Journal of Engineering Sciences, 31/2, 20–27.

[12] JABER A.SH., et al., 2025, *Experimental Investigation of Process Parameters in the Hydrostatic Forming to Enhance a Square Steel Cup Formability*, Tikrit Journal of Engineering Sciences, 32/2, 1–13.

[13] YINGJIAN G., et al., 2025, *A Transfer Learning Method for Deep Drawing Force Prediction of Sheet Metal*, European Journal of Mechanics – A/Solids, 114, 105780.

[14] LAL R.K., CHOUBEY V.K., DWIVEDI J.P., KUMAR S., 2018, *Study of Factors Affecting Springback in Sheet Metal Forming and Deep Drawing Process*, Mater. Today Proc., 5/2, 4353–4358.

[15] VALLASTER E., WIESENMAYER S., MERKLEIN M., 2024, *Effect of a Strain Rate Dependent Material Modeling of a Steel on the Prediction Quality of a Numerical Deep Drawing Process*, Prod. Eng. Res. Devel., 18/1, 47–60.

[16] GONG Y., LOU J., HOU W., SU L., WANG S., DONG L., 2022, *Cold Stamping Forming Simulation and Springback Analysis of High Strength Steel Plate for Automobile Body*, Forest Chemicals Review, 1177–1187.

[17] RIGAS N., SCHMID H., MERKLEIN M., 2021, *Comparison of Different Forming Methods on Deep Drawing and Springback Behavior of High-Strength Aluminum Alloys*, IOP Conf. Series: Materials Science and Engineering, 1157/1.

[18] GABRIEL M., et al., 2025, *Design of Multi-Step Dies for Sheet Metal Forming Using a Workpiece-Performance-Based Approach: a Preliminary Study*, MATEC Web of Conferences, 408/01085.

[19] Abaqus/Explicit 3DEXPERIENCE R2017X, Dassault Systemes SIMULIA Corp. 1301 Atwood Avenue, Suite 101W Jonhston, RI 02919, USA.

[20] JIRATHEARANAT S., et al., 2004, *Hydroforming of Y-Shapes – Product and Process Design Using FEA Simulation and Experiments*, Journal of Materials Processing Technology, 146/1, 124–129.